Electric Power Systems Research 147 (2017) 213–223

Contents lists available at ScienceDirect

Electric Power Systems Research

journal homepage: www.elsevier.com/locate/epsr

Distributed cooperative control of energy storage units in microgrid based on multi-agent consensus method

Chongxin Huang[a,*], Shengxuan Weng[a], Dong Yue[a], Song Deng[a], Jun Xie[b], Hui Ge[b]

[a] Institute of Advanced Technology, Nanjing University of Posts and Telecommunications, Nanjing 210023, China
[b] College of Automation, Nanjing University of Posts and Telecommunications, Nanjing 210023, China

ARTICLE INFO

Article history:
Received 30 August 2016
Received in revised form 24 February 2017
Accepted 26 February 2017

Keywords:
Distributed cooperative control
Multi-agent method
Energy storage unit
Microgrid

ABSTRACT

For a grid-connected microgrid, volatile renewable resources and undulating loads lead to the active power fluctuation at the point of common coupling (PCC), which brings extra regulation burden to the main power system. This paper proposes a distributed cooperative control method to regulate the charging/discharging behavior of multiple energy storage units (ESUs) to restrain the active power fluctuation at the PCC. With the proposed method, all the ESUs operate in the same state of charge (SoC) and ratio of power (RoP), and thus the uneven degradation of ESUs is avoided. Under the distributed control architecture, the network resource can be saved since the control center just communicates with parts of ESUs. The simulations are performed on a typical microgrid, and the effectiveness of the proposed method is validated by numerous results.

1. Introduction

In the past decades, energy storage technologies have drawn much attention and become to play an important role in large-scale power systems, since they have great potential to improve the security, stability and economy of power system operation [1]. Nowadays, there are various storage technologies used in power systems, such as electrochemical storage (e.g. lead-acid battery, Li-ion battery and nickel-metal-hydride battery), electrical storage (e.g. super-capacitor storage and super-conducting storage), mechanical storage (e.g. flywheel storage and pumped hydraulic storage) and thermal storage (e.g. sensible heat storage and latent heat storage) [2]. Each storage technology has its own advantages and disadvantages. In general, cost and capacity demand are two main factors for choosing the type of energy storage systems. For instance, the electrochemical storage is a good candidate to enhance the flexibility of the microgrid, since it has favorable characteristics in energy absorption/release and fast dynamic response, meanwhile, its cost and capacity are acceptable for microgrid operator [3].

In recent years, renewable generation has been developed fast as the increasing environmental awareness. In particular, renewable microsources, such as photovoltaic units and small-capacity wind turbines, have been applied to power generation far and wide [4,5]. As we know, the renewable resources with variability and uncertainty bring great challenge to power system operation [6]. Microgrids as a small-scale generation and distribution system usually integrates a cluster of distributed generators (DGs), energy storage units (ESUs) and loads [7]. In deregulated electricity market, microgrids are allowed to participate in ancillary services (such as power support and demand response) to gain additional income. In order to facilitate their market participation, microgrid operators have to coordinate the DGs, ESUs and loads reasonably. In the long-time scale, the optimal bidding and operational strategy is formulated to maximize the profits in hour-ahead (or day-ahead) electricity market. In the real-time scale, the distributed resources of the microgrid are controlled to respond to the real-time power command from the market contract or the dispatching schedule [8].

In general, a microgrid has two primary modes of operation, namely islanded mode and grid-connected mode [9–11]. In islanded mode, the supply-demand balance must be locally maintained. ESUs are usually used to balance the loads and the renewable energies through charging or discharging power [10]. In grid-connected mode, the microgrid needs to take charge of buffering the unbalance between the loads and the renewable energies, and provides ancillary service to main power grid [11,12]. In both of two modes, the coordination for multiple ESUs is crucial to microgrid operation.

Recently, many studies have been carried out to coordinate multiple distributed resources in microgrid. In centralized control mode, a central controller is needed to coordinate all the ESUs

* Corresponding author.
E-mail address: huangchongxin@foxmail.com (C. Huang).

http://dx.doi.org/10.1016/j.epsr.2017.02.029
0378-7796/

Nomenclature

A. Acronyms

ESU	energy storage unit
PCC	point of common coupling
SoC	state of charge
RoP	ratio of power
DG	distributed generator
WT	wind turbine
PV	photovoltaic
DC	direct-current

B. Sets and matrices

$\mathcal{G}$	undirected graph
$\mathcal{V}$	node set of graph $\mathcal{G}$
$\mathcal{E}$	edge set of graph $\mathcal{G}$
$\mathcal{A}$	weighted adjacent matrix of graph $\mathcal{G}$
a_{ij}	element of $\mathcal{A}$; $a_{ij} > 0$ if $(i, j) \in \mathcal{E}$, and $a_{ij} = 0$ otherwise
$\mathcal{L}$	Laplacian matrix of graph $\mathcal{G}$
ℓ_{ij}	element of $\mathcal{L}$; $\ell_{ii} = \sum_{j=1, j\neq i}^{n} a_{ij}$ and $\ell_{ij} = -a_{ij}$

C. Parameters

C_i	nominal capacity of ESU i
$V_{\mathrm{dc}i}$	DC voltage of ESU i
$P_{\mathrm{esu}i}^{\max}$	maximum power of ESU i
$K_{\mathrm{soc}i}$	redefined negative constant of ESU i; $K_{\mathrm{soc}i} = -P_{\mathrm{esu}i}^{\max}/(C_i V_{\mathrm{dc}i})$
n	number of ESUs
K_P	positive gain of virtual leader
α, β, γ	parameters of distributed controller

D. Variables

SoC_i	SoC of ESU i
$P_{\mathrm{esu}i}$	active power of ESU i
$P_{\mathrm{esu}i}^{\mathrm{ref}}$	reference active power of ESU i
$Q_{\mathrm{esu}i}$	reactive power of ESU i
$Q_{\mathrm{esu}i}^{\mathrm{ref}}$	reference reactive power of ESU i
P_{pcc}	active power at the PCC
$P_{\mathrm{pcc}}^{\mathrm{ref}}$	reference active power at the PCC
$I_{\mathrm{dc}i}$	DC current of ESU i
s_i	SoC of ESU i; $s_i = SoC_i$
s_i'	redefined variable of ESU i; $s_i' = s_i/K_{\mathrm{soc}i}$
p_i	RoP of ESU i
s_0	consensus SoC for all the ESUs
p_0	consensus RoP for all the ESUs
u_i	input signal of the inserted integrator for ESU i

[13,14]. Under hierarchical control framework [15–17], multi-level decision architecture is used to deal with distributed energies and ESUs. However, the aforementioned centralized mode and hierarchical mode need a control center to communicate with each distributed resource, as well as a powerful central controller to perform the complicated computation [18].

As the penetration level of small-capacity distributed resources increases, the centralized or hierarchical mode will be encountered with intractable problems on communication and computation [19]. Instead, a distributed control mode which uses the local communication and computation is a preferable solution to deal with the coordination problems of the large-scale small-capacity resources [20]. In [21], a distributed control scheme with high reliability and low-bandwidth communication is proposed to ensure proportional load sharing and improve voltage quality in DC microgrid. In [22], in order to keep the frequency and voltage stable, a distributed networked algorithm is used to design the secondary control in droop-controlled microgrid. The aforementioned methods [19–22] are applied to coordinating the DGs rather than the ESUs.

Based on the distributed control architecture, some control strategies have been used to coordinate multiple ESUs. In [23], a distributed algorithm is utilized to regulate the power of multiple ESUs to provide ancillary services for power systems. In [24], a distributed model predictive control (MPC) scheme is presented to coordinate the ESUs for voltage regulation. Similarly, the distributed MPC scheme is also used to cope with the optimization problem of ESUs to keep supply-demand balance and maintain voltage and frequency stability [25]. However, the distributed methods in [23–25] ignore the state of charge (SoC) balance of ESUs, which may result in the overcharging and overdischarging actions of ESUs.

At aspect of the SoC balance of ESUs, at a long-time scale, the authors in [26] use a localized control strategy to regulate the SoC of each ESU to avoid depletion or saturation of ESUs. In [27], the authors present a new MAS-based decentralized control architecture for the energy management of a microgrid. In [28], a fully distributed control strategy based on mean field games is proposed for the management of micro-storage devices. The above control methods for SoC balance need the long-time-scale predicted data from load prediction and DG power prediction, which tends to generate some inevitable uncertainties. So, it is difficult for these methods to achieve the SoC balancing in real-time scale. For the real-time SoC balancing, the authors in [29] present an energy sharing scheme for controlling the SoC of a energy storage system with multiple battery cells. The authors in [30] design a distributed cooperative control scheme for the dynamic energy balancing between the energy storage devices to improve frequency regulation and reliability of microgrid. The authors in [31] use an adaptive droop control method to govern the SoC of each ESU in DC microgrid. In [32], a multi-agent cooperative control strategy is proposed to coordinate the power sharing between the heterogeneous energy storage devices and the SoC balancing between the batteries in DC microgrid. However, the control methods about SoC balancing in [31,29,30,32] have not been applied to providing the auxiliary services for main power grid, such as tracking the power command from main power grid and mitigating the power fluctuation at the PCC of microgrid.

Toward a grid-connected microgrid, this paper proposes a distributed cooperative control method based on second-order multi-agent system to govern the charging/discharging behavior of multiple ESUs. By the proposed method, firstly the relation between the SoC and the ratio of power (RoP) of each ESU is described to be a second-order dynamic serving as a follower. Then, a virtual leader is constructed to generate the desired SoC and RoP for all the ESUs. By this way, the coordination problem of multi-ESU system is turned into designing control algorithm for a second-order multi-agent system. Based on the second-order multi-agent model, a distributed coordination method is adopted to design controllers for all the ESUs. The designed controllers can make all the ESUs converge to the same SoC and RoP, and enable the total power of the microgrid to track the power command from the main power grid. Furthermore, the designed cooperative controller has preferable robustness and scalability.

Compared with the existing work on the control of multi-ESU system in microgrid, the main contributions of this paper can be outlined as follows:

(1) To alleviate the power balancing burden of main power grid, the ESUs are used to smooth the active power fluctuation at the PCC and respond to the active power command from the main power grid.

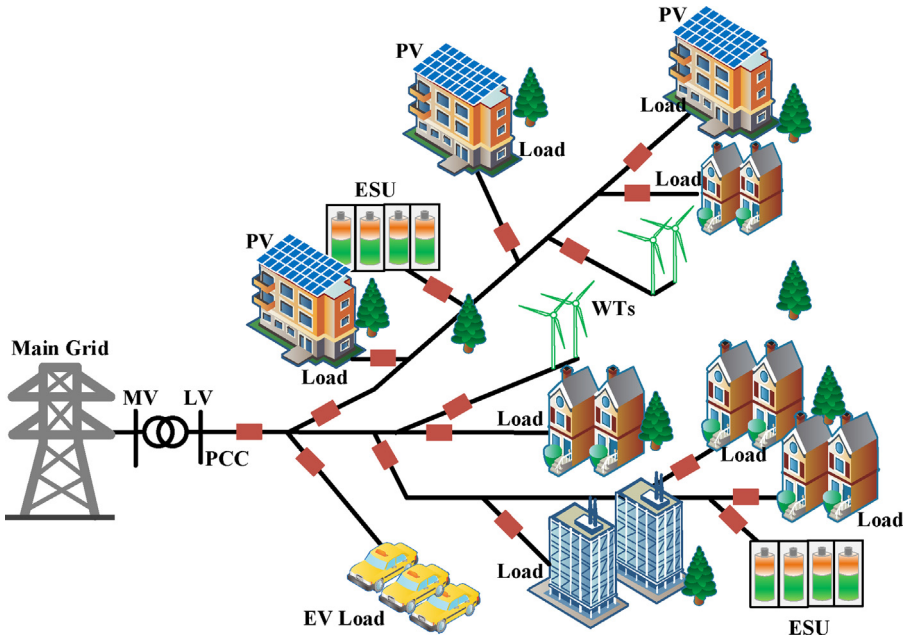

Fig. 1. Configuration of a microgrid.

(2) Under distributed control frame, a leader-following second-order dynamic model is established for the control problem of multi-ESU system. The established dynamic model is simple for the control algorithm design.
(3) A distributed tracking control via a variable structure approach is adopted to design the cooperative algorithm for the multi-ESU system. The designed algorithm makes all the ESUs reach a consensus on the SoC and RoP, meanwhile, the total active power of the microgrid is regulated to its reference value.
(4) A typical microgrid test system is built to perform the real-time dynamic simulation. Simulation results indicate that the expected objectives and performances are attained under the distributed cooperative control.

2. Problem formulation

The configuration of a microgrid shown in Fig. 1 consists of residential loads, wind turbine (WT) generators, photovoltaic (PV) generators and ESUs. The microgrid is connected to the main power grid through an MV/LV transformer at the point of common coupling (PCC). As we know, the loads fluctuate with the change of power demand, and WT power and PV power are also volatile due to the local weather variation. Therefore, the power flow at the PCC fluctuates frequently, which causes much adverse influence on power system operation. In this case, the effective regulation of multiple ESUs is a good choice to mitigate the power flow fluctuation.

In this paper, WT and PV generators in the microgrid always operate in the maximum power output mode, while ESUs are used to smooth the active power fluctuation of microgrid and respond to the active power command from main grid. To guarantee the uninterrupted power regulation capability of the ESUs, the microgrid operator needs to control the SoC so as to avoid the depletion and saturation of ESUs. In addition, the fair utilization of the ESUs is also an important issue that we concerned. The same RoP and SoC of each ESU is not only a practical way to reach the fair utilization and load balancing, but also an effective measure to avoid the uneven degradation of ESUs.

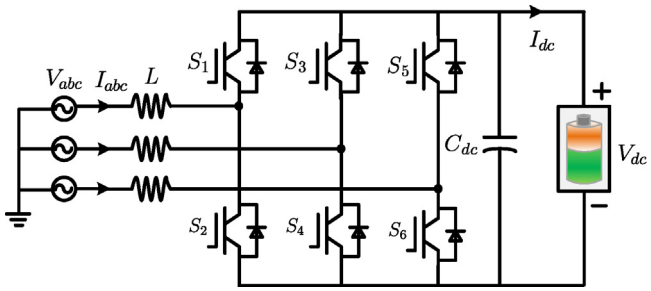

Fig. 2. Configuration of the ESU AC/DC converter.

2.1. Review of ESU converter control

A three-phase boost converter shown in Fig. 2 is often used for charging or discharging an ESU. The converter topology consists of six insulated-gate bipolar transistors (IGBTs) with antiparallel diodes, three boost inductors on the AC side to filter the harmonic current, and a capacitor on the DC side to form a DC voltage.

This paper adopts a typical dual-loop decoupling control scheme presented in [33] to control the three-phase boost converter. The control algorithm shown in Fig. 3 can regulate the active power P and the reactive power Q, respectively. The controller has two input signals, namely, the reference active power P^{ref} and the reference voltage V^{ref}. Here, the reactive power Q is utilized to control the voltage of the node where the ESUs are inserted, and thus the reference voltage V^{ref} serves as an input instead of the reference reactive power Q^{ref}. Since the local control of ESU is not the focus of this paper, the details about the control algorithm are ignored. If needed, one can refer to the literature [33].

2.2. Dynamic model of multi-ESU system

The main concern of this paper is to design a distributed cooperative control strategy to maintain the total active power balance in the microgrid and make all the SoC and RoP of the ESUs reach consensus. In essence, this issue is about how to formulate the reference power P^{ref} for each ESU to achieve the above objectives based on the dynamic model of multi-ESU system.

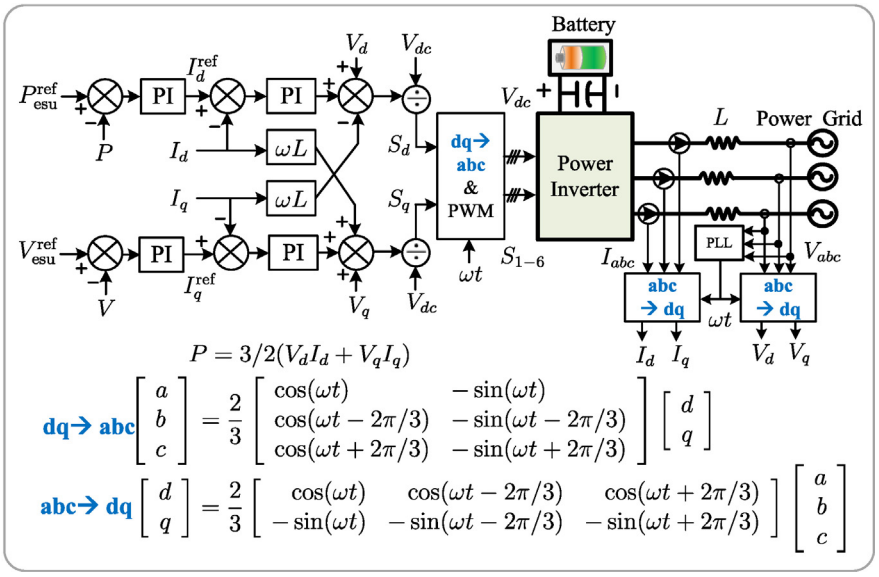

Fig. 3. Control of the bidirectional ESU charger.

Generally, the SoC of an ESU with electrochemical batteries can be described by the coulomb counting method as follows [34]:

$$SoC_i = SoC_i(t_0) - \frac{1}{C_i}\int_{t_0}^{t} I_{\mathrm{dc}i}\,dt \tag{1}$$

where $SoC_i(t_0)$ denotes the initial value of SoC at t_0; C_i denotes the nominal capacity of the ESU; $I_{\mathrm{dc}i}$ denotes the DC current of the ESU; subscript i denotes the ith ESU, similarly hereinafter.

By ignoring the power loss of ESU inverter, according to the power balance, the power of an ESU can be expressed as

$$P_{\mathrm{esu}i} = V_{\mathrm{dc}i} I_{\mathrm{dc}i} \tag{2}$$

where $P_{\mathrm{esu}i}$ denotes the power of the ESU (power flow direction: from ESU to microgrid), and $V_{\mathrm{dc}i}$ denotes the DC voltage of the ESU.

By substituting (2) into (1), it yields

$$SoC_i = SoC_i(t_0) - \frac{1}{C_i}\int_{t_0}^{t} \frac{P_{\mathrm{esu}i}}{V_{\mathrm{dc}i}}\,dt \tag{3}$$

According to the converter control of ESU, it can be known that the local dual-loop decoupling scheme shown in Fig. 3 can make the active power track its reference value in short time. Based on this fact, the active power of ESU can be deemed to be equal to its reference power ($P_{\mathrm{esu}i} = P^{\mathrm{ref}}_{\mathrm{esu}i}$). In order to adjust the active power of the ESUs dynamically to achieve the control objective of the microgrid, an integrator ($1/s$) is inserted in front of the reference power signal $P^{\mathrm{ref}}_{\mathrm{esu}i}$. Thus the active power dynamic of the ith ESU is described as

$$\dot{P}^{\mathrm{ref}}_{\mathrm{esu}i} = u_i \tag{4}$$

where u_i is the input signal of the inserted integrator.

Dividing Eq. (4) by the maximum power of the ith ESU, it yields

$$\frac{\dot{P}^{\mathrm{ref}}_{\mathrm{esu}i}}{P^{\mathrm{max}}_{\mathrm{esu}i}} = \frac{u_i}{P^{\mathrm{max}}_{\mathrm{esu}i}} \tag{5}$$

By defining an virtual input $\mu_i = u_i/P^{\mathrm{max}}_{\mathrm{esu}i}$ and the RoP of ESU $p_i = P^{\mathrm{ref}}_{\mathrm{esu}i}/P^{\mathrm{max}}_{\mathrm{esu}i}$, the dynamic equation (5) can be modified to be

$$\dot{p}_i = \mu_i \tag{6}$$

According to the SoC equation (3), the relation between the SoC and the RoP of an ESU can be described by a dynamic equation. By defining $s_i = SoC_i$ and differentiating (3) with respect to time t, it yields

$$\dot{s}_i = -\frac{1}{C_i V_{\mathrm{dc}i}} P_{\mathrm{esu}i} = -\frac{P^{\mathrm{max}}_{\mathrm{esu}i}}{C_i V_{\mathrm{dc}i}} p_i = K_{\mathrm{soc}i} p_i \tag{7}$$

where $K_{\mathrm{soc}i} = -P^{\mathrm{max}}_{\mathrm{esu}i}/(C_i V_{\mathrm{dc}i})$. In general, the voltage of electrochemical batteries $V_{\mathrm{dc}i}$ drops with the SoC decrease, but the voltage drops much slower than the SoC. If the batteries of ESUs do not operate at the depletion and saturation state, $V_{\mathrm{dc}i}$ varies in a small range. Since $V_{\mathrm{dc}i}$ variation is slow and small, $V_{\mathrm{dc}i}$ is assumed to be a constant [34]. With the above assumption, $K_{\mathrm{soc}i}$ is deemed constant to simplify the dynamic model of ESU and facilitate the subsequent controller design. Supposing that all the ESUs in the microgrid are homogeneous, we have $K_{\mathrm{soc}1} = K_{\mathrm{soc}2} = \cdots = K_{\mathrm{soc}n} = K_{\mathrm{soc}}$.

By combining (6) and (7), we can obtain the dynamic model for n ESUs as follows:

$$\begin{aligned} \dot{s}_i &= K_{\mathrm{soc}} p_i \\ \dot{p}_i &= \mu_i \end{aligned} \quad (i = 1, 2, \ldots, n) \tag{8}$$

or

$$\begin{aligned} \dot{s}'_i &= p_i \\ \dot{p}_i &= \mu_i \end{aligned} \quad (i = 1, 2, \ldots, n) \tag{9}$$

where $s'_i = s_i/K_{\mathrm{soc}}$, and n denotes the number of ESUs.

2.3. Control objectives of multi-ESU system

In this paper, the cooperative control is designed to realize the consensus on the SoC and RoP of the ESUs. This means that the following equations hold:

$$\begin{aligned} &s_1 = s_2 = \cdots = s_n = s_0 \\ &p_1 = p_2 = \cdots = p_n = p_0 \end{aligned} \tag{10}$$

or

$$\begin{aligned} &s'_1 = s'_2 = \cdots = s'_n = s'_0 \\ &p_1 = p_2 = \cdots = p_n = p_0 \end{aligned} \tag{11}$$

where s_0 and p_0 are the given values of the SoC and the RoP, respectively; $s'_0 = s_0/K_{\mathrm{soc}}$.

In addition, to restrain the power fluctuation at the PCC and response to the dispatching command from the main power system, the designed cooperative control strategy should guarantee that the total active power of the microgrid is equal to its reference power, namely

$$P_{\text{pcc}} = P_{\text{pcc}}^{\text{ref}} \tag{12}$$

where P_{pcc} and $P_{\text{pcc}}^{\text{ref}}$ are the active power and the reference active power at the PCC, respectively. Here, the direction of the active power is from the main grid to the microgrid.

It can be seen from (9) that the dynamics of multi-ESU system are represented by a second-order multi-agent model. In the following section, the cooperative control will be designed to realize the objectives shown in (11) and (12).

Remark: In this paper, the ESUs are used to make the total power of the microgrid track the reference power command from the dispatching schedule. All the ESUs running in the same SoC and RoP in the steady state means that the ESUs are utilized fairly. In other words, each ESU has the same load rate and charge/discharge cycles in a certain period of time. This kind of operation mode can realize load balancing and avoid the uneven degradation of multiple ESUs. On contrary, the ESUs running in different SoC and RoP (e.g. some ESUs running in the heavy-load state, while the others running in light-load state) results in load unbalancing, which will lead to uneven degradation (ESUs aging unevenly). It should be noted that all the ESUs having the same SoC and RoP may not be an effective operational mode when they are used for other regulation requirements (such as load shifting).

3. Distributed cooperative control algorithm

Toward the problems formulated in Section 2, a distributed cooperative control method based on variable structure approach is adopted to design a high-level control strategy for each ESU to generate the reference active power command next.

3.1. Graph theory preliminary [35]

In a multi-agent system, information exchange among the agents can be described by a topological graph. Assuming a multi-agent system with n agents, we use a weighted undirected graph $\mathcal{G} = (\mathcal{V}, \mathcal{E}, \mathcal{A})$ to model the interaction among these agents, where, $\mathcal{V} = \{1, 2, \ldots, n\}$ denotes the node set; $\mathcal{E} = \mathcal{V} \times \mathcal{V}$ denotes the edge set; and $\mathcal{A} = [a_{ij}] \in \mathbb{R}^{n\times n}$ denotes the weighted adjacent matrix. An edge (i, j) in $\mathcal{G}$, namely $(i, j) \in \mathcal{E}$, means that agent i and agent j are neighbors, and thus they can obtain information from each other. The weighted adjacent matrix $\mathcal{A}$ of graph $\mathcal{G}$ is defined such that the element a_{ij} is a positive weight if $(i, j) \in \mathcal{E}$, and $a_{ij} = 0$ otherwise. In the undirected graph $\mathcal{G}$, we have $a_{ij} = a_{ji}$. Here Laplacian matrix $\mathcal{L} = [\ell_{ij}] \in \mathbb{R}^{n\times n}$ of graph $\mathcal{G}$ is defined as: $\ell_{ii} = \sum_{j=1, j\neq i}^{n} a_{ij}$ and $\ell_{ij} = -a_{ij}, i \neq j$. Note that $\mathcal{L}$ is symmetric positive semi-definite, and has a simple zero eigenvalue with an associated eigenvector (an all-one column vector), and all other eigenvalues are positive if and only if $\mathcal{G}$ is connected.

3.2. Distributed cooperative controller design

3.2.1. Design virtual leader

The problem (11) can be solved through realizing the consensus of multi-ESU system represented by the second-order dynamic model (9). To solve the active power balancing problem (12), a virtual leader shown in Fig. 4 is designed for the multi-ESU system. The virtual leader consists of two series integrators. The first one is used to generate the reference RoP (p_0) via the integral of the deviation between the reference power $P_{\text{pcc}}^{\text{ref}}$ and the real power P_{pcc} at the PCC of microgrid. The second one is used to generate the reference SoC (s_0') via the integral of the RoP p_0. The state variables (s_0' and p_0) of the virtual leader are sent to some of the ESUs (followers) for trajectory tracking in the distributed control.

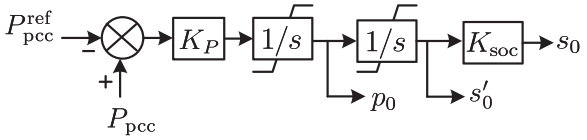

Fig. 4. Control for determining the desired SoC and RoP.

The dynamics of the virtual leader shown in Fig. 4 can be written as follows:

$$\begin{aligned} \dot{s}_0' &= p_0 \\ \dot{p}_0 &= K_P(P_{\text{pcc}} - P_{\text{pcc}}^{\text{ref}}) \end{aligned} \tag{13}$$

where K_P is a given positive gain. It should be noted that the total power of a real microgrid is always bounded. In other words, $|\dot{p}_0| \leq \psi$, where ψ is a positive constant.

3.2.2. Design distributed control algorithm

According to the virtual leader shown in (13), it is obvious that p_0 is time-varying in a dynamic process. To obtain excellent performances, a distributed tracking control via variable structure approach is adopted to design a cooperative algorithm for each ESU (called follower). This control scheme can make all the followers track the trajectory of the virtual leader.

The cooperative algorithm is as follows [35]:

$$\begin{aligned} \mu_i = \frac{u_i}{P_{\text{esui}}^{\max}} &= -\sum_{j=0}^{n} a_{ij}[(s_i' - s_j') + \alpha(p_i - p_j)] \\ &\quad - \beta \,\text{sgn}\left(\sum_{j=0}^{n} a_{ij}[\gamma(s_i' - s_j') + (p_i - p_j)]\right) \end{aligned} \tag{14}$$

where a_{ij} is the (i, j)th entry of the adjacency matrix $\mathcal{A}$; a_{i0} is a positive constant if the ith follower can receive the information (s_0 and p_0) from the virtual leader, and $a_{i0} = 0$ otherwise; α, β and γ are positive constants; sgn$(\cdot)$ denotes a sign function. During the control algorithm design, we resort to the following lemma and theorem.

Lemma 1 ([35]). *Suppose that the undirected graph $\mathcal{G}$ is connected and at least one a_{i0} is nonzero. Let*

$$\begin{aligned} E &= \begin{bmatrix} (1/2)M^2 & (\gamma/2)M \\ (\gamma/2)M & (1/2)M \end{bmatrix} \\ F &= \begin{bmatrix} \gamma M^2 & (\alpha\gamma/2)M^2 \\ (\alpha\gamma/2)M^2 & \alpha M^2 - \gamma M \end{bmatrix} \end{aligned} \tag{15}$$

where α and γ are positive constants, and $M = \mathcal{L} + \text{diag}(a_{10}, \ldots, a_{n0})$. If γ satisfies

$$0 < \gamma < \min\left\{\sqrt{\lambda_{\min}(M)}, \frac{4\alpha\lambda_{\min}(M)}{4 + \alpha^2\lambda_{\min}(M)}\right\} \tag{16}$$

then both E and F are symmetric positive definite.

Theorem 1 ([35]). *Suppose that the undirected graph $\mathcal{G}$ is connected and at least one a_{i0} is nonzero. Using (14) for (9), if $\beta \geq \psi$ and γ satisfied (16), then $s_i'(t) \to s_0'(t)$ and $p_i(t) \to p_0(t)$ globally exponentially as $t \to \infty$. In particular, it follows that*

$$\|[\Delta s'^T(t) \quad \Delta p^T(t)]\|_2 \leq \tau_1 e^{-\tau_2 t} \tag{17}$$

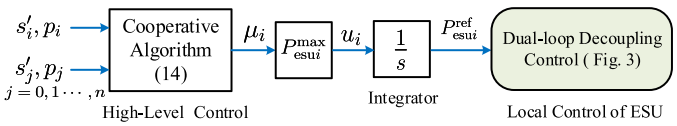

Fig. 5. Structure of the proposed control scheme for the *i*th ESU.

where Δs *and* Δp *are the column stack vectors of* $\Delta s_i' = s_i' - s_0'$ *and* $\Delta p_i = p_i - p_0$ *for* $i = 1, \ldots, n$, *respectively; and* τ_1 *and* τ_2 *can be computed as*

$$\tau_1 = \sqrt{\frac{[\Delta s'^T(0) \quad \Delta p^T(0)]E[\Delta s'^T(0) \quad \Delta p^T(0)]^T}{\lambda_{\min}(E)}}$$
$$\tau_2 = \frac{\lambda_{\min}(F)}{2\lambda_{\max}(E)} \tag{18}$$

where E and F are defined in Lemma 1.

For saving pages, the proof processes for Lemma 1 and Theorem 1 are ignored in this paper. More details about the proof processes can be found in [35].

According to Theorem 1, in order to guarantee the convergence of the cooperative algorithm shown in (14), the communication network and control parameters should satisfy the following requirements:

1) The communication graph $\mathcal{G}$ is connected.
2) At least one a_{0i} is nonzero in the adjacency matrix $\mathcal{A}$.
3) The parameter β satisfies $\beta \geq \psi$.
4) The parameter γ satisfies the inequality (16).

By combining the high-level distributed cooperative control with the local dual-loop decoupling control of the boost converter, the whole control for multi-ESUs system can be achieved and shown in Fig. 5. Here, the integrator ($1/s$) is inserted between the high-level control and the local control to generate the first-order dynamic shown in Eq. (4), which is used for adjusting the active power of the ESUs dynamically.

3.2.3. Analyze closed-loop system

The closed-loop system consists of the communication networks, the distributed cooperative controller, and the microgrid (control plant). As stated in Part II, the objectives of the closed-loop system are to achieve the consensus SoC and RoP of the ESUs shown in (10) and to meet the active power balance requirement of the microgrid shown in (12). From the distributed control algorithm (14) based on Theorem 1, we can know that all the ESUs converge to the same SoC and RoP ($s_i' \to s_0'$ and $p_i \to p_0$, where $s_i' \to s_0'$ means $s_i \to s_0$) through selecting appropriate parameters for the distributed controller. Therefore, the first objective in (10) can be attained. For the second objective in (12), it can be explained as: according to the virtual leader shown in Fig. 4, if the total input power from the main grid is bigger than the reference power ($P_{pcc} > P_{pcc}^{ref}$), then the virtual leader will increase p_0 and send it to some ESUs to raise their (p_i), which results in decrease of P_{pcc} from the main grid until the power balance is satisfied ($P_{pcc} = P_{pcc}^{ref}$). Similarly, if $P_{pcc} < P_{pcc}^{ref}$, the RoP of all the ESUs will decrease correspondingly until $P_{pcc} = P_{pcc}^{ref}$. From the above explanation we can see that the objective in (12) can also be attained.

Here it should be noted that the convergence of the closed-loop system is related to the connectivity of the communication network graph $\mathcal{G}$. Generally, the more communication channels mean the faster convergence rate, but leading to the higher communication cost [36]. Therefore, it is necessary to make a compromise between the connectivity and the economic issue during the communication network design.

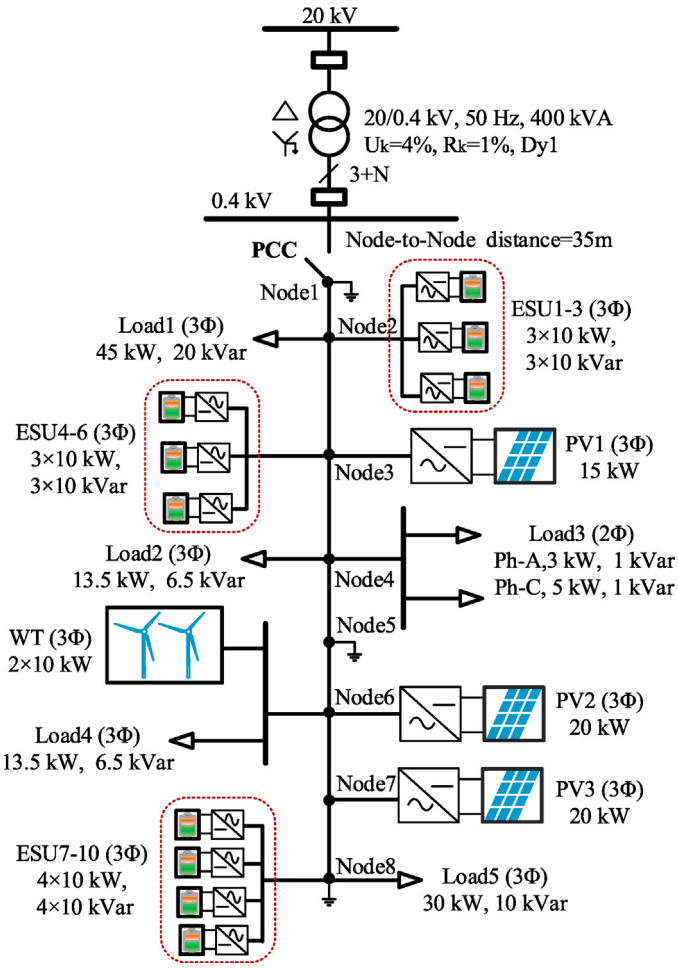

Fig. 6. Single-line diagram of the microgrid test system.

4. Case studies

4.1. Description of simulation system

To verify the proposed distributed cooperative control method, the simulations are performed by using MATLAB/SimPowerSystems tool. The microgrid test system shown in Fig. 6 is derived from a benchmark LV network which is developed in the EU project "Microgrid" [37]. The microgrid includes 3 PVs, 2 WTs, 5 loads and 10 ESUs. The capacities of the loads, the PVs, the WTs and the ESUs shown in Fig. 6 denote their rated values.

In this paper, it is assumed that all the ESUs with nickel-metal-hydride batteries have the same rated capacity, rated power and charging/discharging characteristics. These ESUs are divided into three groups and installed on Node 2, Node 3 and Node 8, respectively. The maximum charging/discharging power of each ESU is set to be $P_{esui}^{max} = 10$ kW. The battery parameters of the 10 ESUs for the simulations are listed in Table 1. It should be noted that the battery capacity is scaled down to 1/10 (4 Ah) of its practical value (40 Ah) in order to illustrate the change of the SoC clearly.

According to the cooperative control method, this paper designs a communication topology for 10 ESUs with a virtual leader shown in Fig. 7. The topology shows that the communication between the virtual leader and the ESUs is unidirectional (e.g. $\alpha_{02} = 1$, but $\alpha_{20} = 0$), and the communication between two ESUs is bidirectional (e.g. $\alpha_{12} = \alpha_{21} = 1$). Here, in order to enhance the reliability of the communication with the virtual leader, we design three

Table 1
Parameters of nickel-metal-hydride batteries.

Parameters	Values
Nominal voltage	500 V
Fully charged voltage	560 V
Rated capacity	4 Ah
Maximum capacity	4.3 Ah
Capacity at nominal voltage	3.8 Ah
Nominal discharge current	20 A
Internal resistance	1.25 Ω

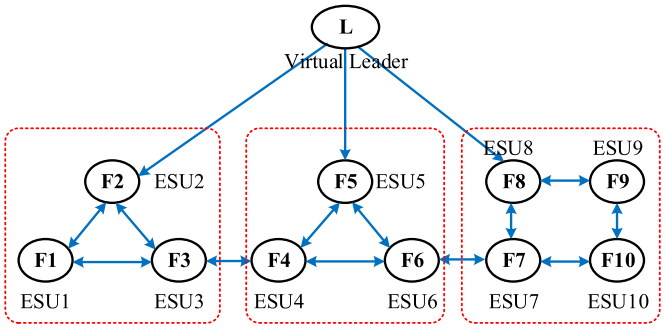

Fig. 7. Communication topology for 10 ESUs with a virtual leader.

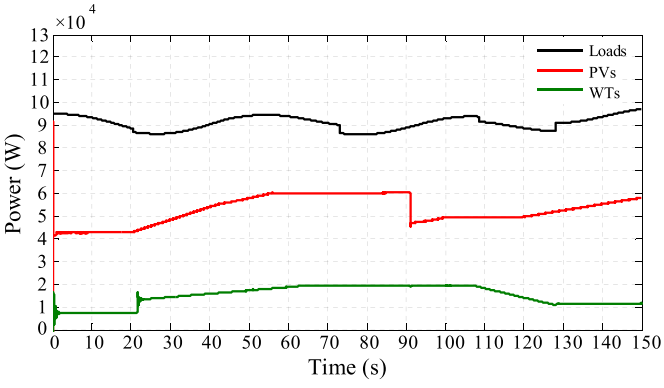

Fig. 8. Active power of loads, PVs and WTs.

communication links between the virtual leader and the followers. In this way, the distributed control system can continue working when one or two communication links fail.

In the simulations, the parameters of the virtual leader at PCC are selected as: $K_P = 0.0001$, $p_0^{\max} = 1$, $p_0^{\min} = -1$, $s_0^{\max} = 1$, $s_0^{\min} = 0.2$. The controller parameters in (14) for each ESU are chosen as: $\alpha = 5$, $\beta = 20$, $\gamma = 1$.

4.2. Analysis of simulation results

4.2.1. Case I: normal operation of microgrid

In the first case, we test the performances of the proposed control scheme in keeping the active power balance and achieving the same SoC and RoP for multiple ESUs. In the simulation, the initial SoC of the 10 ESUs is set as: $[s_1, s_2, s_3, \ldots, s_{10}] = [48.0\,\%, 48.5\,\%, 49.0\,\%, \ldots, 52.5\,\%]$. The initial SoC of the virtual leader is assumed to be $s_0(0) = 50.0\%$. The reference power command from the main grid is set as: at $t = 0$ s, $P_{\text{pcc}}^{\text{ref}} = 0$ kW; at $t = 50$ s, $P_{\text{pcc}}^{\text{ref}} = 40$ kW; at $t = 100$ s, $P_{\text{pcc}}^{\text{ref}} = -10$ kW. The reference voltages of the nodes with ESUs are required to maintain 1 pu, namely $V_2^{\text{ref}} = V_3^{\text{ref}} = V_8^{\text{ref}} = 1$ pu. The active power curves of the loads, the PVs and the WTs are shown in Fig. 8.

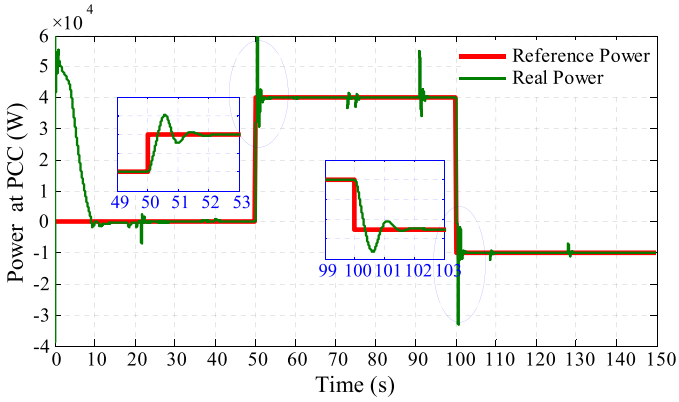

Fig. 9. Active power at PCC of microgrid in Case I.

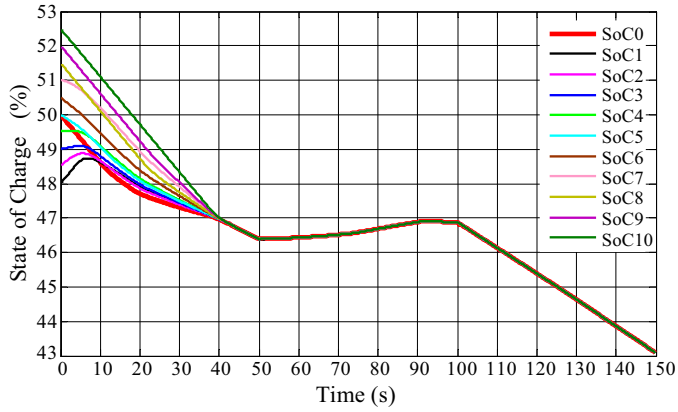

Fig. 10. SoC of virtual leader and 10 ESUs in Case I.

The dynamic responses for Case I are shown in Figs. 9–12, where the subplots embedded in the figures are the partial magnified views.

Fig. 9 shows that the total active power P_{pcc} of the microgrid tracks the power command $P_{\text{pcc}}^{\text{ref}}$ very well whether the microgrid absorbs the power from the main power grid or feeds the power to the main power grid. Furthermore, the settling time of the closed-loop control system is quite short. Consequently, we can see that the proposed distributed control for the ESUs can regulate the active power at the PCC effectively, and thus the microgrid is able to provide the auxiliary services to the main power grid.

Seeing the SoC responses in Fig. 10 and the RoP responses in Fig. 11, we can find that all the ESUs keep the pace with the virtual leader after 40 s, namely, each ESU has the same SoC and RoP as the leader. Thus, the microgrid operator can obtain the SoC and RoP of all the ESUs by observing the virtual leader alone. Moreover, the identical SoC and RoP can avoid unnecessary charging or discharging among the ESUs.

The reactive power of ESUs is used to regulate the voltage of the nodes with the ESUs. The voltage curves of Node 2, 3 and 8 are shown in Fig. 12. It is indicated that the ESUs make the voltages at Node 2, 3 and 8 be equal to the desired value (1 pu) in steady state, and even maintain the voltage in a small range ($1 \pm 0.5\%$ pu) in dynamic process.

4.2.2. Case II: disconnection/reconnection of ESUs

In the second case, we test the ability of the proposed distributed cooperative controller to accommodate the disconnection/reconnection of an ESU. In the simulation, the active power of the loads, PVs and WTs, as well as the initial SoC of the virtual leader and the ESUs in Case II are the same as that in Case I; the reference voltage of Node 2, 3 and 8 is also 1 pu; and the reference

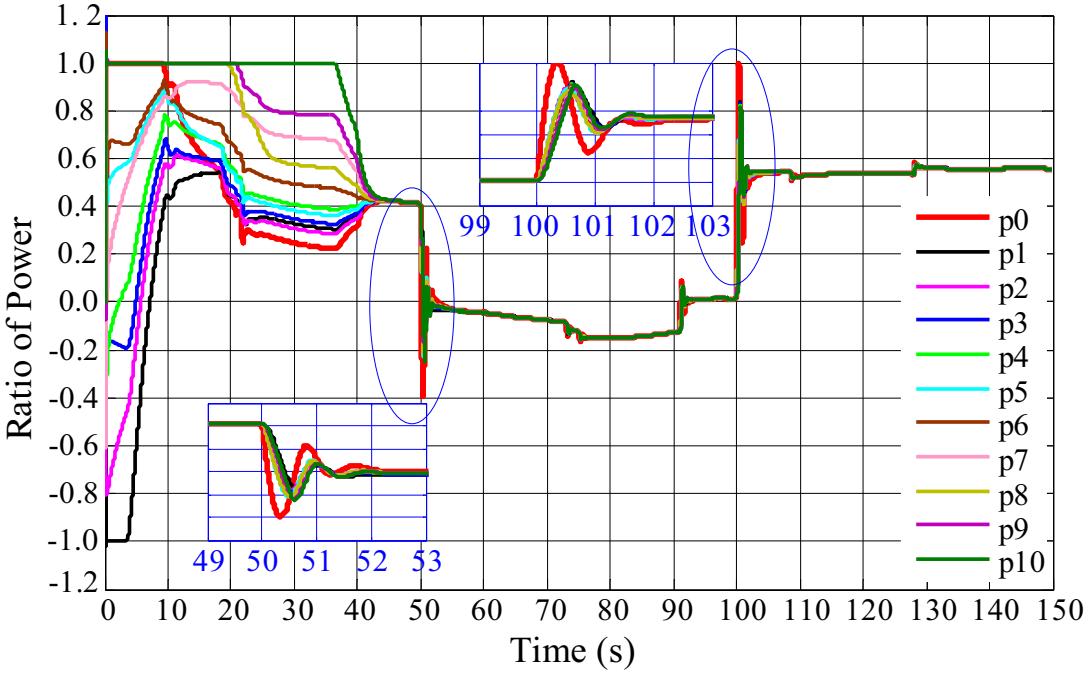

Fig. 11. RoP of virtual leader and 10 ESUs in Case I.

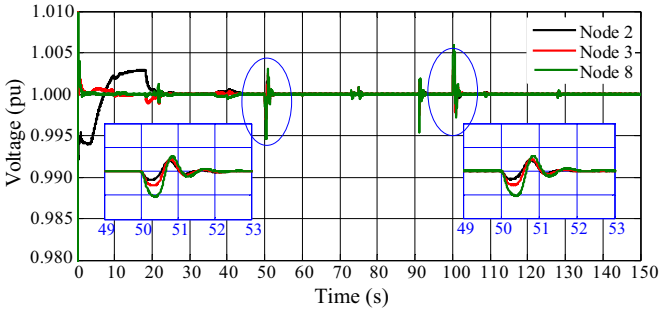

Fig. 12. Voltage at Node 2, 3 and 8 in Case I.

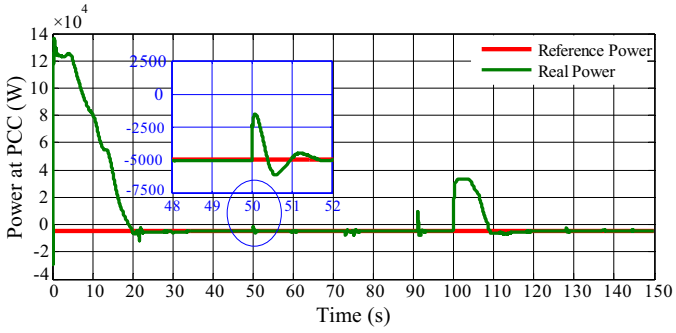

Fig. 13. Active power at PCC of microgrid in Case II.

active power of the microgrid is kept constant ($P_{pcc}^{ref} = -5$ kW) all the time. The simulation sequence for the disconnection/reconnection of an ESU is set as follows:

- At $t = 0$ s, all the ESUs are integrated into the microgrid with the communication topology shown in Fig. 7.
- At $t = 50$s, ESU2 is disconnected from the microgrid, and the communication linked to ESU2 is interrupted, namely, $a_{02} = 0$, $a_{21} = a_{12} = 0$, $a_{23} = a_{32} = 0$;
- At $t = 100$ s, ESU2 is reconnected to the microgrid, and the communication is restored to the original topology.

The simulation results for Case II are shown in Figs. 13–16. From the response curves in Fig. 13, it can be observed that the total active power P_{pcc} follows its reference value P_{pcc}^{ref} well, even after an ESU is disconnected from (or reconnected to) the microgrid.

The SoC and RoP responses are plotted in Figs. 14 and 15. In the initial stage ($0 \le t < 50$ s), all the ESUs following the virtual leader are forced to reach the consensuses on the SoC and RoP. At $t = 50$ s, though ESU2 is disconnected from the microgrid, the rest of the ESUs continue operating with the identical SoC and RoP. When ESU2 is reconnected to the microgrid at $t = 100$ s, all the ESUs follow the virtual leader to achieve the identical SoC and RoP again. It should be noted that the reconnecting action of ESU2 at $t = 100$ s

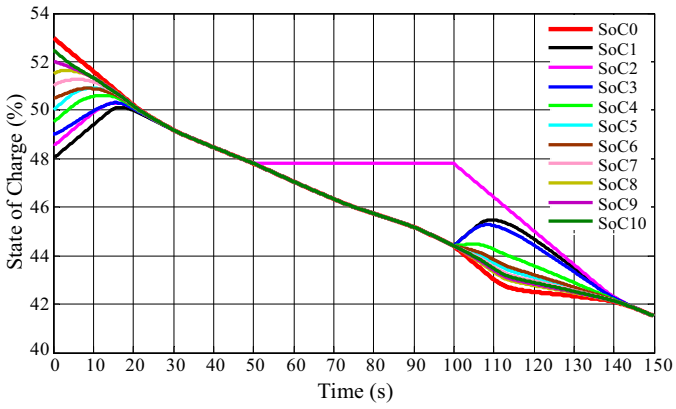

Fig. 14. SoC of virtual leader and 10 ESUs in Case II.

causes larger overshoot and longer settling time than the disconnecting action at $t = 50$ s. The reason is that after ESU2 is reconnected to the microgrid at $t = 100$ s, all the ESUs need to readjust their active power by a large margin to regain the same SoC and RoP with the virtual leader. Consequently, the large power adjustment of the ESUs leads to the large active power change at the PCC of the microgrid.

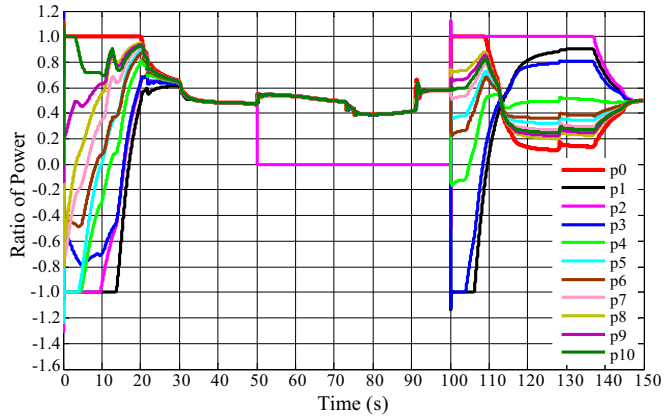

Fig. 15. RoP of virtual leader and 10 ESUs in Case II.

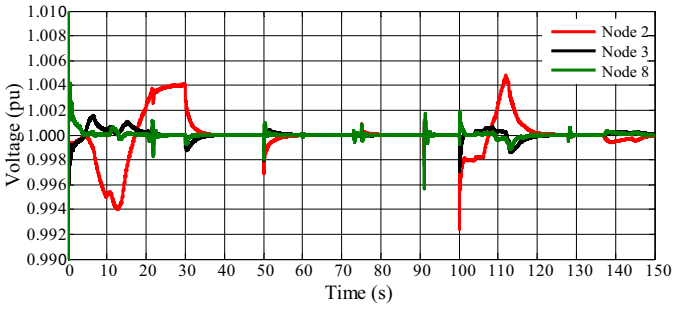

Fig. 16. Voltage at Node 2, 3 and 8 in Case II.

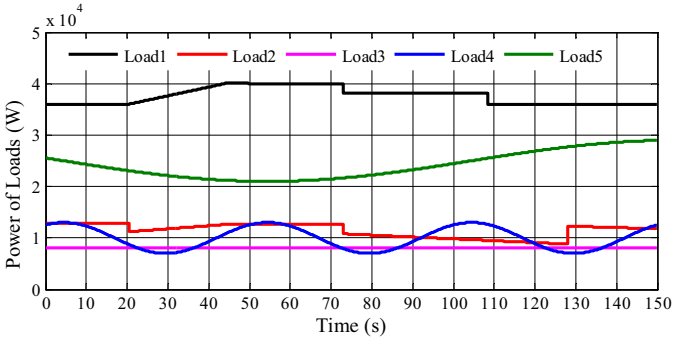

Fig. 17. Active power of loads.

Fig. 16 shows the voltage curves on Node 2, 3, and 8. We can see that the voltage of each node also reaches the desired value (1 pu) in the steady state, and does not exceed the allowed range in dynamic process.

4.2.3. Case III: voltage quality test

Though this paper concerns about the active power control of multi-ESU system in microgrid, it is necessary to observe the voltage profiles of all the nodes of the microgrid since the active power flow may raise voltage quality problem. It should be noted that in the simulation, the reactive power of 10 ESUs is utilized to regulate the node voltages, while the PVs and WTs operate in the unity-power-factor state. In Case III, the active power curves of loads, PVs and WTs are assumed to be fluctuant and shown in Figs. 17–19, the reference value of the active power at the PCC is set to be $P_{pcc}^{ref} = 10\,kW$, and the rest of simulation parameters are the same as the ones in Case I.

For the given active power curves of loads, PVs and WTs shown in Figs. 17–19, the simulation results are plotted in Figs. 20–23.

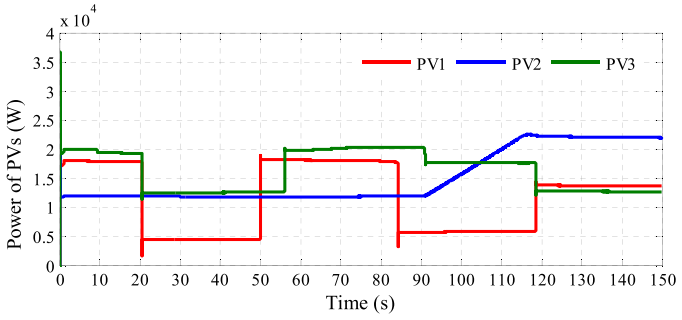

Fig. 18. Active power of PVs.

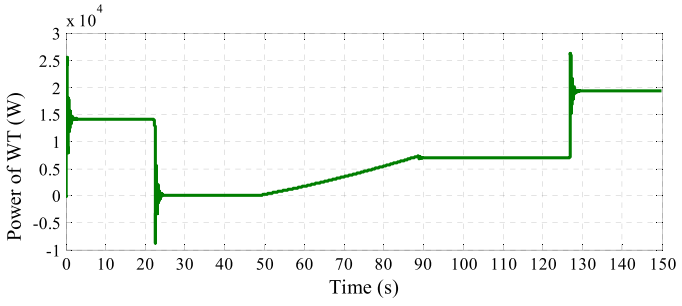

Fig. 19. Active power of WTs.

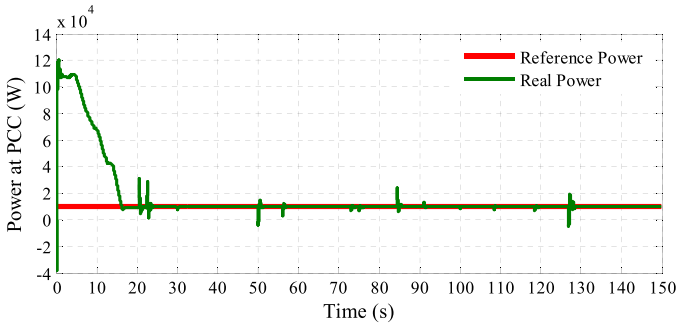

Fig. 20. Active power at PCC of microgrid in Case III.

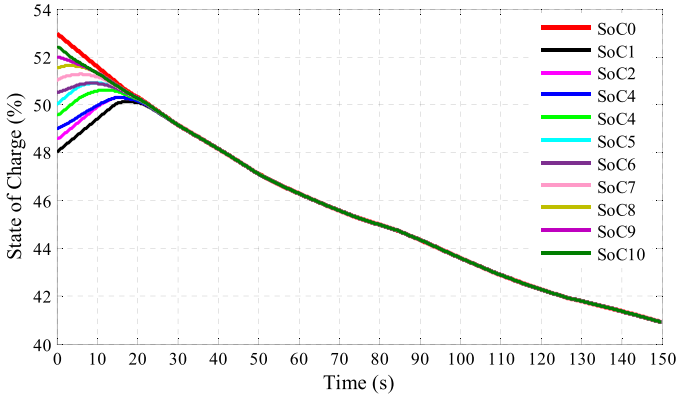

Fig. 21. SoC of virtual leader and 10 ESUs in Case III.

Seeing from Fig. 20, we can find that under the scenario of Case III, the proposed control algorithm can guarantee that the active power at the PCC of the microgrid tracks the reference power command from the main grid even though the active power of loads, PVs and WTs is volatile. Figs. 21 and 22 show that the designed distributed controller makes all the ESUs reach the consensus on SoC and RoP, which contributes to the fair utilization of the ESUs.

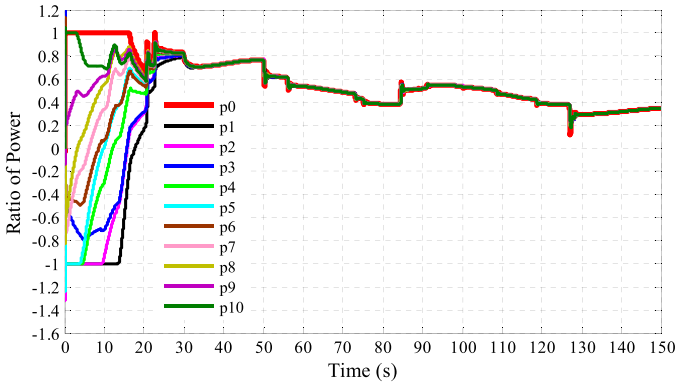

Fig. 22. RoP of virtual leader and 10 ESUs in Case III.

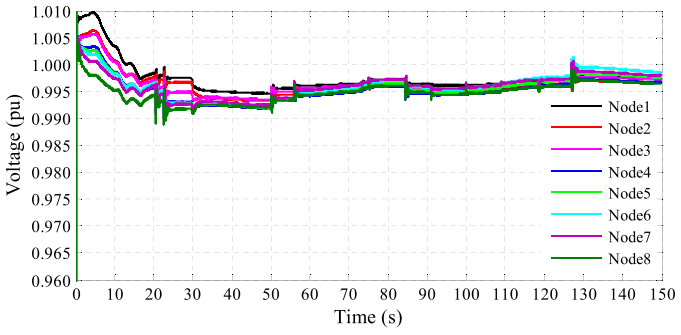

Fig. 23. Voltage of all the nodes in Case III.

Fig. 23 shows that the voltage deviations of all the nodes are controlled in ±1.2% range, which is far less than the allowed maximum deviation (±5%) of the microgrid. Based on the simulation results it can be inferred that using the reactive power of ESUs to regulate the voltage amplitudes of Node 2, 3 and 8 can ensure the voltage profile of all the nodes meet the requirement of voltage quality, since Node 2, 3 and 8 are located in the head, middle and tail of the microgrid feeder.

4.3. Summary of case studies

The above simulation tests indicate that the expected control objectives (tracking the active power command at the PCC and obtaining the identical SoC and RoP) can be achieved via the distributed cooperative control. In addition, the voltage profile delivered to consumers satisfies the requirement of voltage quality under the local converter control of ESUs. Furthermore, the distributed control algorithm can accommodate the disconnection/reconnection of ESUs. In other words, if one or several of the ESUs is connected to (disconnected from) the microgrid, it is not needed to reconfigure their distributed control algorithm on the premise that the communication graph $\mathcal{G}$ is connected. Therefore, we can see that the distributed control strategy has excellent adaptability and scalability.

5. Conclusion

This paper proposes a distributed cooperative control scheme to manage the charging/discharging behavior of ESUs for controlling the active power at the PCC of a grid-connected microgrid. The designed controller can guarantee that all the ESUs converge to the same SoC and RoP. Under the distributed cooperative control, on the one hand the microgrid can response to the power command from the main power system; on the other hand the uneven degradation of the ESUs can be avoided because all the ESUs have identical SoC and RoP. In addition, the distributed controller can cope with the problem on the disconnection/reconnection of ESU. This implies that the control scheme has favorable adaptability and scalability. Moreover, the distributed control mode helps to save the communication cost and reduce the computational burden for the control center of microgrid. Through the simulations with MATLAB/SimPowerSystems on a typical microgrid, the effectiveness of the proposed control scheme is verified.

It should be noted that the proposed distributed cooperative control scheme is designed for the multiple ESUs with the same parameters (homogeneous ESUs). The issue on the cooperative control for multiple heterogeneous ESUs needs to be studied further. In addition, for simplifying the dynamic model of multi-ESU system, V_{dci} variation of ESUs is ignored in this paper, which may lead to some deviations between the simplified model and the real one. The designed cooperative algorithm based on variable structure approach guarantees the convergence and stability of the closed-loop control system. However, to further improve the control performances of multi-ESU system, V_{dci} variation should be considered in the dynamic model. This will be the future work of the authors.

Acknowledgements

This work is supported by National Natural Science Foundation of China (Nos. 51507085, 61533010 and 61503193) and Scientific Found of Nanjing University of Posts and Telecommunications (NUPTSF Grants Nos. NY214202 and XJKY14018).

References

[1] V.A. Boicea, Energy storage technologies: the past and the present, Proc. IEEE 102 (11) (2014) 1777–1794.
[2] S.O. Amrouche, D. Rekioua, T. Rekioua, S. Bacha, Overview of energy storage in renewable energy systems, Int. J. Hydrogen Energy 41 (45) (2016) 20914–20927.
[3] X. Qiu, T.A. Nguyen, M.L. Crow, Heterogeneous energy storage optimization for microgrids, IEEE Trans. Smart Grid 7 (3) (2016) 1453–1461.
[4] Y.W. Li, C.N. Kao, An accurate power control strategy for power-electronics-interfaced distributed generation units operating in a low-voltage multibus microgrid, IEEE Trans. Power Electron. 24 (12) (2009) 2977–2988.
[5] A.M. Bouzid, J.M. Guerrero, A. Cheriti, M. Bouhamida, P. Sicard, M. Benghanem, A survey on control of electric power distributed generation systems for microgrid applications, Renew. Sustain. Energy Rev. 44 (2015) 751–766.
[6] X. Chen, Y. Hou, S. Tan, C. Lee, S.Y.R. Hui, Mitigating voltage and frequency fluctuation in microgrids using electric springs, IEEE Trans. Smart Grid 6 (2) (2015) 508–515.
[7] J.W. Simpson-Porco, Q. Shafiee, F. Dorfler, J.C. Vasquez, J.M. Guerrero, F. Bullo, Secondary frequency and voltage control of islanded microgrids via distributed averaging, IEEE Trans. Ind. Electron. 62 (11) (2015) 7025–7038.
[8] I. Goroohi Sardou, M.E. Khodayar, K. Khaledian, M. Soleimani-Damaneh, Energy and reserve market clearing with microgrid aggregators, IEEE Trans. Smart Grid 7 (6) (2016) 2703–2712.
[9] O. Palizban, K. Kauhaniemi, Hierarchical control structure in microgrids with distributed generation: island and grid-connected mode, Renew. Sustain. Energy Rev. 44 (2015) 797–813.
[10] T. Morstyn, B. Hredzak, G.D. Demetriades, V.G. Agelidis, Unified distributed control for dc microgrid operating modes, IEEE Trans. Power Syst. 31 (1) (2016) 802–812.
[11] E. Liegmann, R. Majumder, An efficient method of multiple storage control in microgrids, IEEE Trans. Power Syst. 30 (6) (2015) 3437–3444.
[12] N. Rezaei, M. Kalantar, Smart microgrid hierarchical frequency control ancillary service provision based on virtual inertia concept: an integrated demand response and droop controlled distributed generation framework, Energy Convers. Manag. 92 (92) (2015) 287–301.
[13] A.G. Tsikalakis, N.D. Hatziargyriou, Centralized control for optimizing microgrids operation, IEEE Trans. Energy Convers. 23 (1) (2008) 241–248.
[14] K. Tan, X. Peng, P. So, Y. Chu, M. Chen, Centralized control for parallel operation of distributed generation inverters in microgrids, IEEE Trans. Smart Grid 3 (4) (2012) 1977–1987.
[15] J.C. Vasquez, J.M. Guerrero, J. Miret, M. Castilla, L.G. De Vicuna, Hierarchical control of intelligent microgrids, IEEE Ind. Electron. Mag. 4 (4) (2010) 23–29.

[16] F. Delfino, R. Minciardi, F. Pampararo, M. Robba, A multilevel approach for the optimal control of distributed energy resources and storage, IEEE Trans. Smart Grid 5 (4) (2014) 2155–2162.
[17] C.S. Karavas, G. Kyriakarakos, K.G. Arvanitis, G. Papadakis, A multi-agent decentralized energy management system based on distributed intelligence for the design and control of autonomous polygeneration microgrids, Energy Convers. Manag. 103 (2015) 166–179.
[18] Y. Xu, W. Zhang, G. Hug, S. Kar, Z. Li, Cooperative control of distributed energy storage systems in a microgrid, IEEE Trans. Smart Grid 6 (1) (2015) 238–248.
[19] H. Xin, Z. Qu, J. Seuss, A. Maknouninejad, A self-organizing strategy for power flow control of photovoltaic generators in a distribution network, IEEE Trans. Power Syst. 26 (3) (2011) 1462–1473.
[20] R.J. Hamidi, H. Livani, S.H. Hosseinian, G.B. Gharehpetian, Distributed cooperative control system for smart microgrids, Electr. Power Syst. Res. 130 (2016) 241–250.
[21] S. Anand, B.G. Fernandes, J. Guerrero, Distributed control to ensure proportional load sharing and improve voltage regulation in low-voltage dc microgrids, IEEE Trans. Power Electron. 28 (4) (2013) 1900–1913.
[22] Q. Shafiee, J.M. Guerrero, J.C. Vasquez, Distributed secondary control for islanded microgrids – a novel approach, IEEE Trans. Power Electron. 29 (2) (2014) 1018–1031.
[23] H. Xin, M. Zhang, J. Seuss, Z. Wang, D. Gan, A real-time power allocation algorithm and its communication optimization for geographically dispersed energy storage systems, IEEE Trans. Power Syst. 28 (4) (2013) 4732–4741.
[24] K. Meng, Z.Y. Dong, Z. Xu, S.R. Weller, Cooperation-driven distributed model predictive control for energy storage systems, IEEE Trans. Smart Grid 6 (6) (2015) 2583–2585.
[25] K. Worthmann, C.M. Kellett, P. Braun, L. Grune, S.R. Weller, Distributed and decentralized control of residential energy systems incorporating battery storage, IEEE Trans. Smart Grid 6 (4) (2015) 1914–1923.
[26] Y. Wang, K. Tan, X. Peng, P. So, Coordinated control of distributed energy storage systems for voltage regulation in distribution networks, IEEE Trans. Power Deliv. 31 (3) (2016) 1132–1141.
[27] M.R.B. Khan, R. Jidin, J. Pasupuleti, Multi-agent based distributed control architecture for microgrid energy management and optimization, Energy Convers. Manag. 112 (2016) 288–307.
[28] A. De Paola, D. Angeli, G. Strbac, Distributed control of micro-storage devices with mean field games, IEEE Trans. Smart Grid 7 (2) (2016) 1119–1127.
[29] W. Huang, J.A. Abu Qahouq, Energy sharing control scheme for state-of-charge balancing of distributed battery energy storage system, IEEE Trans. Ind. Electron. 62 (5) (2015) 2764–2776.
[30] T. Morstyn, B. Hredzak, V.G. Agelidis, Distributed cooperative control of microgrid storage, IEEE Trans. Power Syst. 30 (5) (2015) 2780–2789.
[31] X. Lu, K. Sun, J.M. Guerrero, J.C. Vasquez, L. Huang, State-of-charge balance using adaptive droop control for distributed energy storage systems in DC microgrid applications, IEEE Trans. Ind. Electron. 61 (6) (2014) 2804–2815.
[32] T. Morstyn, B. Hredzak, V.G. Agelidis, Cooperative multi-agent control of heterogeneous storage devices distributed in a DC microgrid, IEEE Trans. Power Syst. 31 (4) (2016) 2974–2986.
[33] M. Kesler, M.C. Kisacikoglu, L.M. Tolbert, Vehicle-to-grid reactive power operation using plug-in electric vehicle bidirectional offboard charger, IEEE Trans. Ind. Electron. 61 (12) (2014) 6778–6784.
[34] Y.S. Kim, E.S. Kim, S.I. Moon, Frequency and voltage control strategy of standalone microgrids with high penetration of intermittent renewable generation systems, IEEE Trans. Power Syst. 31 (1) (2016) 718–728.
[35] Y. Cao, W. Ren, Distributed coordinated tracking with reduced interaction via a variable structure approach, IEEE Trans. Autom. Control 57 (1) (2012) 33–48.
[36] H. Xin, Z. Lu, Y. Liu, D. Gan, A center-free control strategy for the coordination of multiple photovoltaic generators, IEEE Trans. Smart Grid 5 (3) (2014) 1262–1269.
[37] S. Papathanassiou, N. Hatziargyriou, K. Strunz, A benchmark low voltage microgrid network, in: Proceedings of the CIGRE Symposium: Power Systems with Dispersed Generation, Athens, Greece, 2005.